Acta Cryst. (1992). B48, 515–520

Crystallization and Preliminary Data Analysis of Flock House Virus

BY A. J. FISHER, B. R. MCKINNEY, J.-P. WERY* AND J. E. JOHNSON

Department of Biological Sciences, Purdue University, West Lafayette, Indiana 47907, *USA*

(*Received* 20 *August* 1991; *accepted* 3 *January* 1992)

Abstract

Flock House virus, purified from infected cultured *Drosophila* cells, crystallizes into three different forms under identical growth conditions. Two crystal forms grow in the trigonal space group $R3$, both with equivalent cell constants $a = 323.6$ Å, $\alpha = 61.7°$. The difference between the two trigonal crystal forms is 1.1° in the orientation of the virus particle as determined from the rotation function. Early crystal setups grew in one form, while recent crystals grew in the other form. The third space group, which accounts for 5% of the observed crystals and grows with both trigonal forms, is orthorhombic $I222$ with cell parameters $a = 416.7$, $b = 332.1$, $c = 351.2$ Å. The trigonal crystal forms contain one virion per unit cell and the orthorhombic form contains two particles per cell. All three crystal forms diffract X-rays to 2.8 Å resolution.

Introduction

Flock House virus (FHV), which was first isolated from the grass grub *Costelytra zealandica* (white) (Dearing, Scotti, Wigley & Dhana, 1980), belongs to the virus family *Nodaviridae* (Scotti, Dearing & Mossop, 1983). This family is the simplest group of multipartite viruses. Their genome is divided between two messenger sense RNA molecules and codes for only three genes. The only other known examples of single-stranded RNA multipartite viruses are plant viruses. However, plant viral genomes are generally encapsulated in separate particles. Nodavirus RNA1 and RNA2 are incorporated together in a spherical, non-enveloped icosahedral capsid. Nodaviruses mainly infect insects, but the type member of the family, Nodamura virus, infects mammals as well (Newman & Brown, 1973, 1977).

FHV contains one structural protein (α) consisting of 407 amino acids. Protein α assembles to form a provirion consisting of 180 promoters arranged in a $T = 3$ surface lattice. This labile provirion is stabilized by a maturation cleavage in approximately 80% of the α subunits. Protein α cleaves between Asn 363 and Ala 364 to yield peptides β and γ, containing 363 and 44 amino acids respectively (Hosur *et al.*, 1987). Proteolysis is an autocatalytic first-order reaction with a half-life of 4 h and occurs only after protein α assembles into a provirion (Gallagher & Rueckert, 1988). This maturation cleavage is essential to the life cycle of the virus and may be related to cleavage steps in the picornavirus life cycle (Fernandez-Tomas & Baltimore, 1973; Guttman & Baltimore, 1977; Hoey & Martin, 1974).

The structure of black beetle virus (BBV), another member of the *Nodaviridae* family, was solved in our laboratory at 3.0 Å resolution (Hosur *et al.*, 1987). The protomers have an eight-stranded antiparallel β-barrel domain, as is observed in other animal and plant virus subunits. The structure did yield clues to the nature of the maturation proteolysis. The cleavage site can be identified by a break in the electron density after residue Asn 363, and the first 16 residues of γ can be interpreted. The cleavage is on the interior of the virus facing the RNA center. Asp 75, which lies 3.9 Å away from the cleavage site, is conserved among all nodaviruses and is a good candidate for playing a catalytic role (Kaesberg *et al.*, 1990). The BBV structure did not fully reveal the cleavage mechanism or how proteolysis stabilizes the particle.

FHV is 87% identical to BBV in α protein sequence and is serologically related. Nonetheless, FHV displays biological properties that are different from BBV, which have been associated with the capsid protein (Gallagher, 1987). FHV has been extensively studied, both genetically and biophysically (Gallagher & Rueckert, 1988; Kaesberg *et al.*, 1990), and its structure will greatly aid in developing a better understanding of the structure-function relationship in the nodavirus life cycle. Also, infectious RNA can be derived from cDNA copies of the genomic RNA of FHV (Dasmahapatra *et al.*, 1986). Recently, the gene for the capsid protein of FHV has been expressed in a baculovirus system, resulting in the spontaneous assembly of virus-like particles in large quantity (Schneemann & Rueckert, 1991). Such a system is extremely useful for the study of assembly and maturation of FHV particles, but the high-resolution structure is required to exploit the potential of this system.

We report the preparation of three forms of high-quality crystals of FHV that diffract X-rays from a synchrotron radiation source to 2.8 Å resolution. Using a locked-rotation-function algorithm (Tong & Rossmann, 1990), we determined the orientation of

* Present address: Lilly Research Laboratories, Eli Lilly and Company, Indianapolis, Indiana 46285, USA.

0108-7681/92/040515-06$06.00

the icosahedral non-crystallographic symmetry axes and employed the BBV structure oriented in the FHV unit cell to compute initial phases.

Experimental

Virus production

FHV was propagated in *Drosophila* cell line 1 (Schneider, 1972) and purified by sucrose velocity-gradient centrifugation according to a modified procedure described by Friesen, Scotti, Longworth & Rueckert (1980). The cells were lysed by three cycles of freezing and thawing instead of the reported method.

Crystallization

FHV was crystallized by sitting-drop vapor diffusion (McPherson, 1982). The reservoir buffer was 0.01 *M* bis(2-hydroxyethyl)iminotris(hydroxymethyl)methane (Bis-Tris), 0.02 *M* $CaCl_2$, 2.8% (*w*/*v*) polyethylene glycol (PEG), molecular weight 8000, pH 6.0. The drop consisted of 10 μl FHV at 18 mg ml^{-1} in 0.01 *M* Tris.HCl pH 7.2, plus 10–30 μl of reservoir buffer. The dish was sealed and allowed to equilibrate against 13 ml of reservoir buffer at room temperature.

Data collection and processing

Data were collected by oscillation photography on film (oscillation angles of 0.3 and 0.5°) at two synchrotron radiation sources; the National Synchrotron Light Source (NSLS) ($\lambda = 1.220$ Å, crystal-to-film distance = 110 mm), and the Cornell High Energy Synchrotron Source (CHESS) ($\lambda = 1.565$ Å, crystal-to-film distance = 100 mm). We used the program developed by Rossmann to process the films and measure the diffraction intensities (Rossmann, 1979). The crystal orientation matrix was derived from Kim's auto-indexing program (Kim, 1989). The data were scaled and post-refined (Rossmann, Leslie, Abdel-Meguid & Tsukihara, 1979). A locked-rotation-function algorithm was used to determine the orientation of the icosahedral non-crystallographic symmetry (Tong & Rossmann, 1990). The program *PROLSQ* was used to calculate structure factors from the BBV model positioned in the *R*3 cell (Hendrickson, 1985).

Results

Crystal analysis

Rhombohedral crystals grew to 0.7 mm (body diagonal) in three weeks. The crystals rotated plane-polarized light indicating a non-cubic space group and diffracted X-rays to 2.8 Å resolution (Fig. 1). They were sensitive to radiation; multiple exposures from one crystal were achieved if the crystal was translated after each exposure. Most crystals could only be exposed twice. Therefore, conventional crystal-setting procedures could not be used. At least 100 high-quality crystals are required to collect a data set for structure determination. Auto-indexing the diffraction patterns from the rhombohedral crystals resulted in a primitive rhombohedral cell: $a = 325.5$ Å, $\alpha = 61.8°$. The films were processed with the equivalent hexagonal setting: $a = 334.3$, $c = 786.4$ Å. Volume per molecular weight (V_m) calculation (Matthews, 1968) suggests one virus particle per rhombohedral cell (three per hexagonal cell) with a value of 2.70 $Å^3$ $dalton^{-1}$. The particle packing is pseudo cubic close packed ($\alpha = 60°$ would correspond to a face-centered cubic structure). We established the space group as *R*3 and not *R*32 by scaling statistics.

Approximately five percent of the crystals grew as a skewed rhombohedron in the same drop as the rhombohedral crystals. These crystals were orthorhombic *I*222 with lattice constants $a = 416.7$, $b = 332.1$, $c = 351.2$ Å. There are two virus particles in the unit cell ($V_m = 2.64$ $Å^3$ $dalton^{-1}$). Because of the large number of crystals required for virus structure determination and the limited supply of orthorhombic crystals, all subsequent work described involved the trigonal *R*3 crystal in the hexagonal setting.

A partial data set corresponding to 41 oscillation photographs was collected. We used the film-processing program developed by Rossmann (1979) and applied the crystal orientation matrix derived from Kim's auto-indexing program (1989) to measure

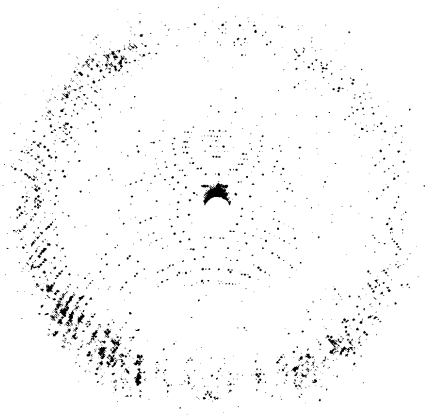

Fig. 1. A 0.5° oscillation photograph taken at CHESS. Wavelength was 1.565 Å, crystal-to-film distance 100 mm, exposure time 160 s. Resolution at film side edges was 3.0 Å. 8771 reflections were accepted for processing of the 14 149 predicted reflections for this film.

Table 1. *Portion of 4σ data collected for two R3 crystal forms*

Resolution range (Å)	FHV *R*3 type I Number of unique reflections	FHV *R*3 type I Percentage of data	FHV *R*3 type II Number of unique reflections	FHV *R*3 type II Percentage of data
∞-20.0	370	18	1033	51
20.0-15.0	852	28	1794	60
15.0-10.0	3579	29	8110	66
10.0-8.0	5153	31	11348	69
8.0-6.0	13981	31	31581	69
6.0-5.0	17543	30	38525	66
5.0-4.0	37849	28	79810	60
4.0-3.5	35316	25	60597	45
3.5-3.0	32407	14	55571	24
Total	147050	23	288369	45
Films	41		101	
R factor* (%)	12.3		11.6	

* R factor $= |\sum_h \sum_i (I_h - I_{hi})/\sum_h \sum_i I_{hi}| \times 100$ where I_h is the mean of the I_{hi} observations of reflection h. Only data for which $I/\sigma(I) \geq 4$ were used.

the diffraction intensity. Using reflections with $I/\sigma(I) \geq 4$, the film data were scaled together with a final scaling R factor of 12.3% (Rossmann *et al.*, 1979). Post-refinement of the data resulted in the convergence of the unit-cell parameters to $a = 331.9$, $c = 782.3$ Å. The unique data collected amounted to 23.1% to 3.0 Å resolution. Table 1 gives a breakdown of data in resolution shells.

Rotation function

The rotation function determines the orientation of the non-crystallographic symmetry relative to the crystal axis (Rossmann & Blow, 1962). Proper orientation is required for placement of the BBV model into the *R*3 cell to compute initial phases for molecular replacement and to average the electron density over non-crystallographic symmetry. Since there is one virion per rhombohedral *R*3 cell, one icosahedral threefold axis must coincide with the crystallographic threefold axis reducing the orientation search to one dimension. This also results in 20-fold non-crystallographic symmetry. A locked-rotation-function program was used to search for the maximum in the R function about the crystallographic threefold axis. This program computes the R function for all non-crystallographic symmetry operators in the 532 point group simultaneously, greatly increasing the power of the rotation function with an incomplete data set (Tong & Rossmann, 1990). The spherical polar coordinate convention used for orienting the rotation vector was defined by Rossmann & Blow (1962) and is illustrated in Fig. 2. The rotation function was computed by rotating the icosahedral symmetry axes about the crystallographic threefold axis by an angle κ and an average R function calculated for the 20 non-crystallographic icosahedral symmetry elements. A broad search was performed for $\kappa = 0$-120° at 4° intervals. The search used 61 large terms ($|F_p|^2 \geq 5 \times |F_h|^2_{avg}$) of the 15 476 measured reflections between 9.0 and 6.0 Å resolution. The radius of integration was 120 Å. One large peak of 5.3σ was observed in the R function at $\kappa = 68°$ (Fig. 3). The precise value of rotation was narrowed down to $\kappa = 68.2°$ incorporating 1135 large terms ($|F_p|^2 \geq 3 \times |F_h|^2_{avg}$).

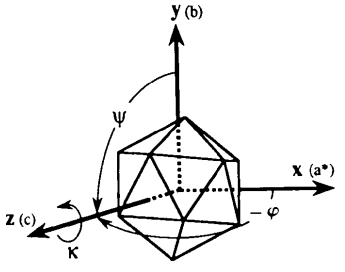

Fig. 2. Spherical polar coordinate convention for orienting the rotation vector displayed with the starting orientation of the icosahedral symmetry elements (at $\kappa = 0°$). An icosahedral threefold axis was positioned along the crystallographic threefold axis (c axis). The rotation vector was fixed along this axis ($\varphi = -90°$, $\psi = 90°$) and a locked rotation function computed for $\kappa = 0$-120°. The orthogonal rotation-function coordinate system is indicated in bold and the hexagonal crystal axes in parentheses.

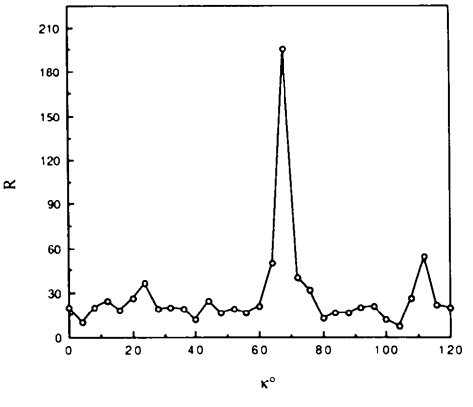

Fig. 3. Locked rotation function of FHV *R*3 type I. The R function was computed from 61 large terms between 9.0 and 6.0 Å resolution as described in the text. φ and ψ were fixed along the crystal threefold axis. The radius of integration was 120 Å.

Recent crystals

Data collected from recent FHV crystals did not scale acceptably with the original 41-film data set. The R factors for the individual films of the new data were over 35% when scaled to the old data set. Both possible hands of the crystal system were tested. The new crystals were rhombohedral and processed as $R3$ with the same unit-cell constants as the previous crystals. This crystal form will be designated FHV $R3$ type II and the crystal of the original data set as FHV $R3$ type I. SDS (sodium dodecyl sulfate) gel electrophoresis of dissolved FHV $R3$ type II crystals resulted in proteins of identical molecular weight to FHV proteins α and β (data not shown). The FHV $R3$ type II data scaled independently of type I data with an R factor of 11.6%. The FHV $R3$ type II data were post-refined and the unit-cell parameters converged to the same values (within estimated errors) as FHV $R3$ type I data. Table 1 shows the amount of data collected at present for both FHV $R3$ types.

We used 970 large terms ($|F_p|^2 \geq 3 \times |F_h|^2_{avg}$) between 9.0 and 6.0 Å resolution to compute a rotation function for the FHV $R3$ type II crystal form. The two crystal $R3$ types differed by a 1.1° particle rotation about the crystallographic threefold axis; type I had a maximum at 68.2°, type II at 67.1° (Fig. 4).

Molecular replacement

The molecular replacement method was used to compute an initial set of phases for the FHV amplitudes. The BBV structure was positioned into the $R3$ type II cell in the same orientation as determined for FHV by the rotation function and initial phases computed. The phasing model consisted of a polyalanine structure of BBV, except for conserved glycines. The program *PROLSQ* (Hendrickson, 1985) was used to calculate structure factors for the phasing model. These structure factors were used to determine the minimum in R factor between the observed and calculated data. The BBV model was oscillated slightly about the threefold axis, from the rotation-function result, and the R factor calculated from 3075 random reflections between 10 and 3.0 Å resolution. The minimum was observed at the same angle ($\kappa = 67.1°$) as the rotation function (Fig. 5). The BBV polyalanine model, oriented from the search described, was used to compute structure factors for all the observed FHV amplitudes resulting in an overall R factor of 47.3% for the initial phasing model. The same real-space orientation test was performed for the FHV $R3$ type I data. The minimum in the R factor correlated with the rotation-function result for the type I data (not shown).

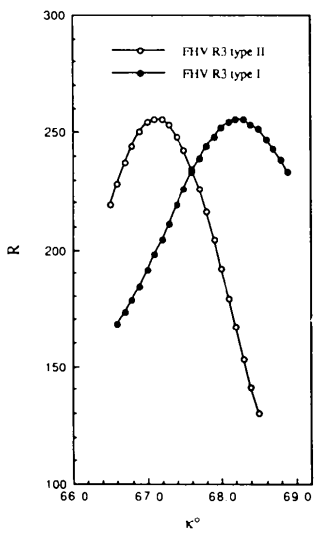

Fig. 4. Locked rotation function of both FHV $R3$ types computed independently of each data set, scaled and plotted together. Conditions are the same as in Fig. 3 except that 1135 large terms were used for FHV $R3$ type I and 970 for type II.

Discussion

The two $R3$ crystal types never grew together, yet the orthorhombic crystal form grew with both trigonal forms. This suggests that a mutation may have arisen on the viral surface that contacts a neighboring particle in the crystal packing for the $R3$ cell but not for the $I222$ cell. The mutation is a conservative substitution because the virus still propagates, assembles and crystallizes in the same space group; only a slight shift in orientation is observed. The mutation could have arisen because of the many infections and purifications required over a period of time to generate the large quantities of virus. Such a mutation was observed in extended passages of human rhinovirus 14 in which an isoleucine was changed to a leucine (Arnold & Rossmann, 1990). Fig. 6 is a packing

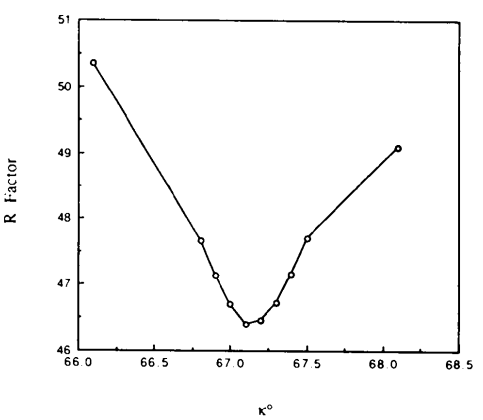

Fig. 5. R factor as a function of particle orientation (κ), comparing observed FHV data to the data calculated using the BBV phasing model (φ and ψ are fixed along the crystal threefold axis). The search used 3075 random reflections between 10.0 and 3.0 Å resolution.

diagram of FHV *R*3 type II in the hexagonal cell. The viral quasi-twofold axes from neighboring particles contact each other and the threefold axis from one virus contacts the fivefold axis of a neighbor. The program used to generate the packing diagram could not resolve any dissimilarity between the two *R*3 types because of the small (1.1°) rotational difference. In the *I*222 cell, the threefold axis of one particle comes close to the threefold axis of its nearest neighbor (not shown). Another possibility for the difference in orientation between the two *R*3 types is the variation in some intrinsic property during crystallization. However, data were collected from both *R*3 crystal types grown in a number of crystallization setups, indicating the change would have to exist in all the later crystal setups.

Only 45.3% of the data to 3.0 Å resolution have been collected for FHV *R*3 type II. More data are currently being collected and processed. Once phases have been calculated for the complete data set, molecular replacement can be started at relatively high resolution (4.0 Å) because of the high similarity between BBV and FHV. The electron density will be averaged over the 20-fold non-crystallographic symmetry to refine the phases.

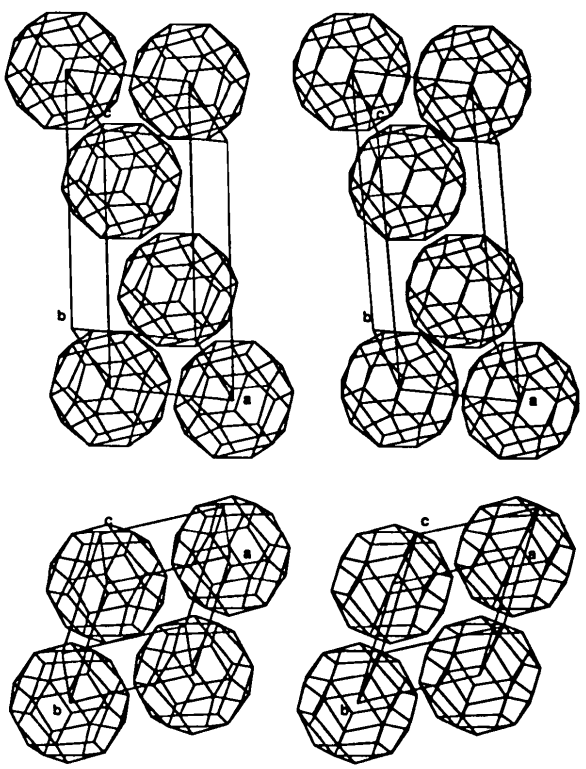

Fig. 6. Stereoview packing diagram of FHV *R*3 type II, showing two different planes of particles in the hexagonal cell (axes labeled). Radius of particles is 160 Å. Lines connect the icosahedral fivefold axis to the threefold axis. Midpoint of lines has icosahedral quasi-twofold symmetry. True twofold axis is vector bisecting two fivefold or threefold axes. The particle packing is pseudo cubic close packed.

The long-term goal of this project is the structural analysis of provirions and a variety of mutants that affect assembly, RNA packaging and cell binding. Many mutants of this type will prevent infectivity (*e.g.* cleavage of the capsid-protein precursor appears to be required for infection), thus the available infectious clone has limited use. The baculovirus expression system has proven to be an excellent way to express cloned genes at high levels in a eukaryotic cell (Luckow & Summers, 1988). The coat proteins for both bluetongue virus and poliovirus that are expressed in this system assemble into non-infectious particles that have the same size and appearance as the authentic virions (French, Marshall & Roy, 1990; Urakawa *et al.*, 1989). A similar result has now been obtained by Schneemann & Rueckert (1991) with the capsid-protein gene for FHV. We have obtained crystals of virus-like particles produced in *Spodoptera frugiperda* cells infected with the baculovirus construct provided by Schneemann & Rueckert, and these are indistinguishable from crystals of native virus. In addition, Schneemann & Rueckert have now mutated the Asn 363/Ala 364 cleavage site to Asp/Ala, which prevents the cleavage and stops maturation at the provirion stage. Crystallization studies with the provirion are underway. The structures of both the native virus and provirion will reveal considerable information on the mechanism of cleavage and how this results in particle stability.

We thank Anette Schneemann and Roland Rueckert for many helpful discussions during the course of this work and especially for providing the baculovirus constructs for the production of the virus-like particles of FHV prior to publishing their results. Liang Tong is gratefully acknowledged for help with the rotation-function analysis. We also thank Zhongguo Chen and Sanjeev Munshi for their help with computer programs. This work is supported by grant GM34220 from the National Institutes of Health. Diffraction data were collected at the Cornell High Energy Synchrotron Source and at Brookhaven National Laboratory in the Biology Department single-crystal diffraction facility at beamline X12-C in the National Synchrotron Light Source. NSLS is supported by the US Department of Energy, Office of Health and Environmental Research.

References

ARNOLD, E. & ROSSMANN, M. G. (1990). *J. Mol. Biol.* **211**, 763-801.

DASMAHAPATRA, B., DASGUPTA, R., SAUNDERS, K., SELLING, B., GALLAGHER, T. & KAESBERG, P. (1986). *Proc. Natl Acad. Sci. USA*, **83**, 63-66.

DEARING, S. C., SCOTTI, P. D., WIGLEY, P. J. & DHANA, S. D. (1980). *N. Z. J. Zool.* 7, 267-269.

FERNANDEZ-TOMAS, C. B. & BALTIMORE, D. (1973). *J. Virol.* **12**, 1122-1130.
FRENCH, T. J., MARSHALL, J. J. A. & ROY, P. (1990). *J. Virol.* **64**, 5695-5700.
FRIESEN, P. D., SCOTTI, P. D., LONGWORTH, J. & RUECKERT, R. R. (1980). *J. Virol.* **35**, 741-747.
GALLAGHER, T. M. (1987). PhD thesis, Univ. of Wisconsin, Madison, USA.
GALLAGHER, T. M. & RUECKERT, R. R. (1988). *J. Virol.* **62**, 3399-3406.
GUTTMAN, N. & BALTIMORE, D. (1977). *J. Virol.* **23**, 363-367.
HENDRICKSON, W. A. (1985). In *Methods in Enzymology*, Vol. 115, edited by H. W. WYCKOFF, C. H. W. HIRS & S. N. TIMASHEFF, pp. 252-270. New York: Academic Press.
HOEY, E. & MARTIN, S. (1974). *J. Gen. Virol.* **24**, 515-524.
HOSUR, M. V., SCHMIDT, T., TUCKER, R. C., JOHNSON, J. E., GALLAGHER, T. M., SELLING, B. H. & RUECKERT, R. R. (1987). *Proteins Struct. Funct. Genet.* **2**, 167-176.
KAESBERG, P., DASGUPTA, R., SGRO, J.-Y., WERY, J.-P., SELLING, B. H., HOSUR, M. V. & JOHNSON, J. E. (1990). *J. Mol. Biol.* **214**, 423-435.
KIM, S. (1989). *J. Appl. Cryst.* **22**, 53-60.
LUCKOW, V. A. & SUMMERS, M. D. (1988). *Biotechnology*, **6**, 47-55.
MCPHERSON, A. JR (1982). *Preparaion and Analysis of Protein Crystals.* New York: Wiley.
MATTHEWS, B. W. (1968). *J. Mol. Biol.* **33**, 491-497.
NEWMAN, J. F. E. & BROWN, F. (1973). *J. Gen. Virol.* **21**, 371-384.
NEWMAN, J. F. E. & BROWN, F. (1977). *J. Gen. Virol.* **38**, 83-95.
ROSSMANN, M. G. (1979). *J. Appl. Cryst.* **12**, 225-238.
ROSSMANN, M. G. & BLOW, D. M. (1962). *Acta Cryst.* **15**, 24-31.
ROSSMANN, M. G., LESLIE, A. G. W., ABDEL-MEGUID, S. S. & TSUKIHARA, T. (1979). *J. Appl. Cryst.* **12**, 570-581.
SCHNEEMANN, A. & RUECKERT, R. (1991). Personal communication, Univ. of Wisconsin, Madison, USA.
SCHNEIDER, I. (1972). *J. Embryol. Exp. Morphol.* **27**, 353-365.
SCOTTI, P. D., DEARING, S. C. & MOSSOP, D. W. (1983). *Arch. Virol.* **75**, 181-189.
TONG, L. & ROSSMANN, M. G. (1990). *Acta Cryst.* A**46**, 783-792.
URAKAWA, T., FERGUSON, M., MINOR, P. D., COOPER, J., SULLIVAN, M., ALMOND, J. W. & BISHOP, D. H. L. (1989). *J. Gen. Virol.* **70**, 1453-1463.

Acta Cryst. (1992). B**48**, 520–531

Structure Determination of a Dimeric Form of Erabutoxin-b, Crystallized from a Thiocyanate Solution

BY P. SALUDJIAN*† AND T. PRANGÉ‡

Chimie Structurale Bio-moléculaire (URA 1430 CNRS), UFR Biomédicale, 93012-Bobigny CEDEX, France

J. NAVAZA

Laboratoire de Physique, Faculté de Pharmacie, 92290-Chatenay-Malabry, France

R. MÉNEZ

Laboratoire d'Ingéniérie des Protéines, CEN Saclay, 91191-Gif sur Yvette CEDEX, France

AND J. P. GUILLOTEAU, M. RIÈS-KAUTT AND A. DUCRUIX

Institut de Chimie des Substances Naturelles, CNRS, 91198-Gif sur Yvette CEDEX, France

(*Received* 22 *September* 1991; *accepted* 21 *January* 1992)

Abstract

Erabutoxin-b, $M_r = 6861.1$, a single 62 amino-acid chain folded by four disulfide bridges, was crystallized in a new orthorhombic form by using thiocyanate as crystallizing agent. The space group is $P2_12_12_1$ with $a = 53.36$ (4), $b = 40.89$ (4), $c = 55.71$ (5) Å, $V = 121\,533.1$ Å^3 and $Z = 8$. X-ray diffraction data were recorded at the LURE synchrotron facility ($\lambda = 1.405$ Å). The structure was solved by molecular replacement and shows a dimeric association through an anti-parallel β-sheet around the twofold non-crystallographic axis. The two independent molecules, one SCN^- ion and 97 associated water molecules were refined by molecular dynamics and annealing techniques to $R = 19.6\%$ (10 913 F_{obs}, resolution 5–1.7 Å). The thiocyanate ion is located at the interface of the dimer and close to the non-crystallographic twofold axis.

Introduction

Crystal nucleation and growth are greatly affected by the type of salt used as the crystallizing agent. In a study of the influence of salts on solubility, it has

* Author to whom correspondence should be addressed.
† E-mail addresses: PS and TP at prange@frlure51; JN at ucba000@frors31; JPG, MRK and AD at ducruix@fricsn51
‡ Alternative address: LURE Bâtiment 209d, Université Paris-Sud, 91405-Orsay CEDEX, France.

0108-7681/92/040520-12$06.00